Thermo X
https://doi.org/10.70401/tx.2026.0033

Supplementary information

Revealing the origin of strongly temperature-dependent lattice thermal conductivity in Cu_2SnSe_3

Hongwei Ming, Zongxuan Lin, Shike Xu, Yunpeng Zheng, Zhong-Zhen Luo, Zhigang Zou

1. Experimental Methods

Sample synthesize: Polycrystalline Cu_2SnSe_3 sample was synthesized by melting under vacuum. Elemental Cu (3N), Sn (5N), and Se (5N) powders (Alfa Aesar) were accurately weighed according to the nominal composition and sealed in quartz tubes. The evacuated quartz tubes were slowly heated to 1193 K in a furnace and held for 8 h, then cooled to 973 K and maintained for 48 h, followed by natural cooling to room temperature.

X-Ray diffraction: Phase identification was performed at room temperature using a Rigaku Miniflex600 powder X-ray diffractometer equipped with Ni-filtered Cu Kα radiation (40 kV, 15 mA). Rietveld refinement was performed with the GSAS II software.

Raman spectroscopy: Raman spectra were collected from 93 K to 773 K with a DXR 3 Flex Raman Spectrometer.

2. Computational Methods

Crystal orbital Hamiltonian population (COHP): The COHP for monoclinic Cu_2SnSe_3 was calculated using the Vienna ab initio Simulation Package (VASP)[1] combined with LOBSTER code.[2] The monoclinic Cu_2SnSe_3 structure was first fully optimized within VASP using the projector-augmented wave (PAW) method. The exchange-correlation energy was described using the generalized gradient approximation (GGA) with the Perdew-Burke-Ernzerhof (PBE) functional.[3] Structural optimization and static calculations were performed with an energy convergence criterion of 1×10^{-5} eV/atom and a plane-wave cut-off energy of 400 eV. Based on the static results, the COHP values for Cu-Se and Sn-Se bonds were obtained using LOBSTER.[2]

Phonon properties at 0 K: The harmonic interatomic force constants, phonon dispersions, phonon density of states, and phonon group velocities for cubic ZnSe, cubic Cu_2SnSe_3, cubic Cu_2SnS_3, monoclinic Cu_2SnSe_3, monoclinic Cu_2SnS_3, and orthorhombic Cu_2SnS_3 at 0 K were calculated using VASP and Phonopy[4] code via the finite displacement method. Strict convergence criteria were applied with thresholds set at 10^{-8} eV for energy and 10^{-6} eV/Å for forces, employing a plane-wave cut-off energy of 400 eV. The phonon dispersions of cation-disordered cubic Cu_2SnSe_3 and Cu_2SnS_3 were modeled using special quasirandom structures ($Cu_8Sn_4Se_{16}$ and $Cu_8Sn_4S_{16}$) embedded in the cubic ZnSe lattice. The resulting dispersions were folded back to the first Brillouin zone using the Upho code. The crystal structures shown in Figure 2 and Figure S8 were visualized using VESTA.[5]

Phonon properties at finite temperature: Ab Initio Molecular Dynamics (AIMD) simulations were performed with VASP for a monoclinic Cu_2SnSe_3 supercell ($Cu_{48}Sn_{24}Se_{72}$). First, an isothermal–isobaric (NPT) ensemble simulation was run at 300 K for 2 ps with a 1 fs time step to obtain the lattice parameters at 300 K. Subsequently, an isothermal–isovolume (NVT) ensemble simulation was carried out at 300 K for 40 ps with the same time step. All AIMD calculations employed a plane-wave cut-off of 400 eV and a Γ-only k-point mesh. From the NVT trajectories, the second-, third-, and fourth-order interatomic force constants (IFCs) were extracted using the temperature-dependent effective potential (TDEP) approach.[6] The cut-off radii were set to 10 Å for 2nd-order, 4.5 Å for 3rd-order, and 4 Å for 4th-order IFCs to comprehensively capture relevant atomic interactions. These IFCs obtained at 300 K were then used in the ShengBTE[7] and FourPhonon[8] programs to compute the lattice thermal conductivity, including both three-phonon (3ph) and four-phonon (4ph) scattering contributions. Convergence tests on the AIMD simulation time and the resulting phonon properties (Fig. R1) confirm that simulations lasting 0.5–10 ps are adequately converged for the purposes of this study.

3. **Convergence Tests.**

We performed convergence tests on the Ab Initio Molecular Dynamics (AIMD) simulation time and the resulting phonon properties, as summarized in Figure R1. Figure R1a shows that the total energy of monoclinic Cu_2SnSe_3 at 300 K remains stable over the entire 40 ps trajectory, with only slight fluctuations. The inset structures at 0, 10, and 40 ps show no significant differences. Figures R1b–d further confirm that the phonon dispersions, group velocities, and lattice thermal conductivities extracted from different time intervals are nearly identical, with only negligible variations. These findings confirm that our 10 ps AIMD simulations are adequately converged for this study.

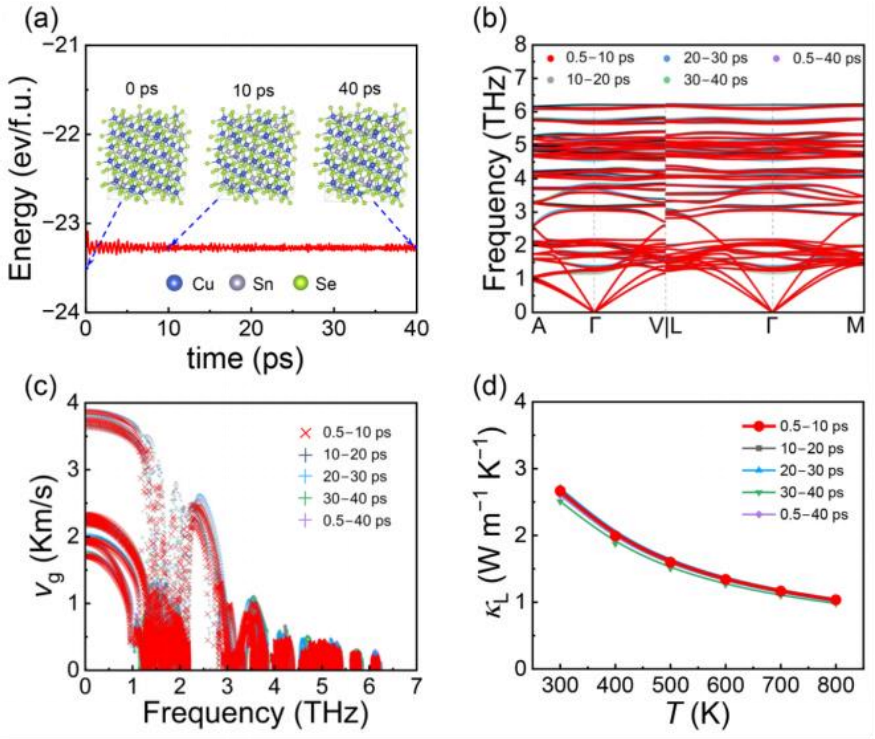

Figure S1. (a) Evolution of the total energy over the entire Ab Initio Molecular Dynamics (AIMD) trajectory of monoclinic Cu_2SnSe_3 at 300 K. The inset displays the supercell configurations at 0, 10, and 40 ps.(b) Phonon dispersions extracted from different time intervals of the AIMD trajectories. (c) Corresponding phonon group velocities derived from the dispersions shown in (b). (d) Lattice thermal conductivities were calculated using the AIMD data from each respective time interval.

4. XRD and Raman Spectra

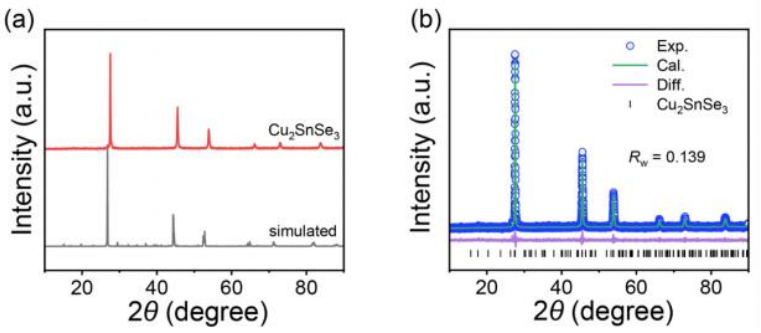

Figure S2. (a) XRD pattern of the synthesized Cu_2SnSe_3. (b) Rietveld refinement of the XRD data, confirming the monoclinic phase.

The role of four-phonon scattering can be experimentally investigated via temperature-dependent Raman spectroscopy by analyzing the shift and broadening of phonon peaks. Within the Klemens–Hart–Aggarwal–Lax model,[9] one phonon decays into two ($\omega_0 \rightarrow \sum \omega_n$, n = 1, 2) or

three ($\omega_0 \rightarrow \sum \omega_m$, n = 1, 2, 3) phonons, gives rise to the following temperature dependences for the frequency (ω_i) and linewidth (Γ_i):

$$\omega_i(T) = \omega_{i0} + A\left(1 + \sum_{n=1}^{2} \frac{1}{e^{\hbar\omega_n/k_BT}-1}\right) + B\left[1 + \sum_{m=1}^{3}\left(\frac{1}{e^{\hbar\omega_m/k_BT}-1} + \frac{1}{\left(e^{\hbar\omega_m/k_BT}-1\right)^2}\right)\right], \quad \text{(S1)}$$

$$\Gamma_i(T) = \Gamma_{i0} + C\left(1 + \sum_{n=1}^{2} \frac{1}{e^{\hbar\omega_n/k_BT}-1}\right) + D\left[1 + \sum_{m=1}^{3}\left(\frac{1}{e^{\hbar\omega_m/k_BT}-1} + \frac{1}{\left(e^{\hbar\omega_m/k_BT}-1\right)^2}\right)\right], \quad \text{(S2)}$$

where $\hbar$ is the reduced Planck constant, k_B is the Boltzmann constant, ω_{i0} and Γ_{i0} are the phonon frequency and linewidth at 0 K, ω_n and ω_m are the frequencies of the phonon participating in the 3ph and 4ph processes, and A, B, C, and D are fitting constants. As demonstrated in previous studies, this approach has successfully verified the four-phonon scattering in diamondoid compounds $AgInSe_2$[10]and $CuInTe_2$.[11]

We synthesized Cu_2SnSe_3 using a vacuum melting method. All diffraction peaks in the X-ray diffraction (XRD) pattern (Figure S2a) can be indexed to the monoclinic phase, and the Rietveld refinement (Figure S2b) confirms the single-phase nature of the obtained material. We measured the Raman spectra of monoclinic Cu_2SnSe_3 from 93 K to 773 K (Figure S3a); selected spectra at representative temperatures are shown in Figure S4b. With increasing temperature, the Raman peaks around 180 cm^{-1} exhibit clear frequency softening (indicated by the red arrow) and become indiscernible above 603 K. However, the calculated Raman spectrum at 300 K (Figure S3c) reveals that this experimental Raman signal actually consists of three overlapping peaks. As a result, it is not possible to extract the temperature-dependent shift and linewidth for each individual component. In addition, the calculated spectrum shows an isolated peak near 60 cm^{-1} (Figure S3c), which is also visible in the experimental spectra (Figures S3a and S3b). Unfortunately, due to a strong fluorescence background in the low-wavenumber region, the signal-to-noise ratio is insufficient to determine the Raman shift and linewidth of this peak accurately.

In view of the above experimental difficulties, we are unable at this stage to provide direct Raman-based evidence supporting the dominant role of four-phonon scattering in our system. Nevertheless, given that previous work on structurally related diamondoid materials $AgInSe_2$[10]and $CuInTe_2$[11] unambiguously demonstrates the significance of four-phonon scattering, it is reasonable to expect that similar scattering processes may also be important here, especially for the temperature dependence of the lattice thermal conductivity κ_L.

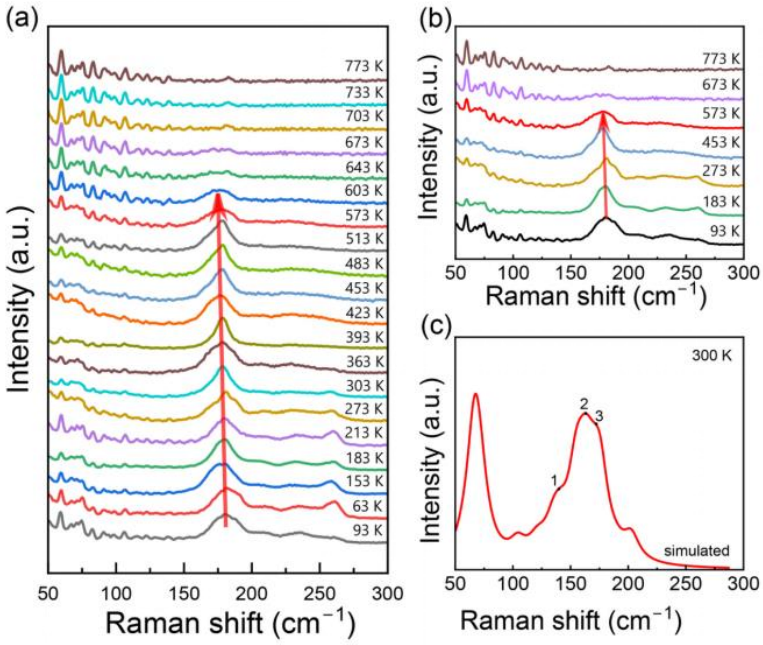

Figure S3. (a) Temperature-dependent Raman spectra of monoclinic Cu_2SnSe_3 measured from 93 K to 773 K. (b) Representative Raman spectra at selected temperatures (93, 183, 273, 453, 573, 673, and 773 K). (c) Calculated Raman spectrum at 300 K.

5. Crystal Orbital Hamiltonian Population

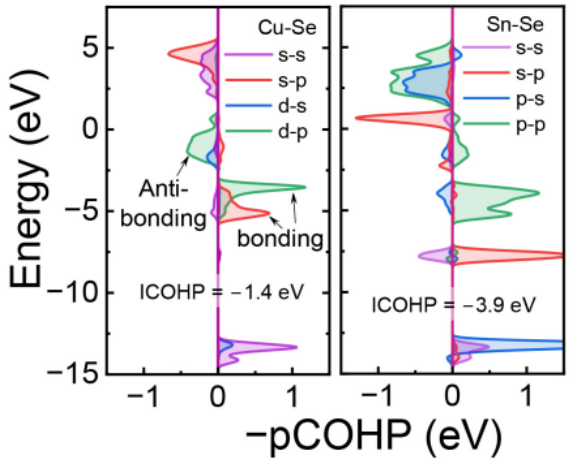

Figure S4. Orbital-projected crystal orbital hamiltonian populations (pCOHP) as a function of energy for Cu-Se and Se-Se bonds; positive and negative −COHP values indicate bonding and antibonding interactions, respectively.

6. Wave-like Coherent Thermal Transport

Figure S5a shows that κ_c accounts for only 3% of the total κ_L at room temperature, but this fraction increases to 15% as the temperature rises to 800 K. Figure S5b displays the spectral κ_c (κ_c^s) as a function of phonon frequency at temperatures from 300 to 800 K for Cu_2SnSe_3. The spectral κ_c profiles closely track the phonon density of states (phDOS), indicating that a higher

phDOS leads to more phonon pairs with similar frequencies, which are the primary drivers of coherent transport. Moreover, with increasing temperature, κ_c^s in the frequency range of 2.5 to 4.5 THz rises noticeably, suggesting that phonon broadening of these optical modes enhances the coherent contribution.

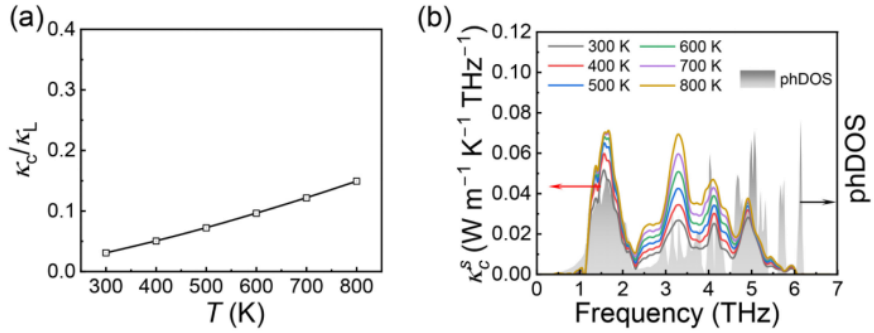

Figure S5. (a) Temperature dependence of the ratio κ_c/κ_L. (b) Spectral κ_c (κ_c^s) as a function of phonon frequency at 300, 400, 500, 600, 700, and 800 K for Cu_2SnSe_3. The gray shaded area represents the phonon density of states.

7. **Phonon Dispersions**

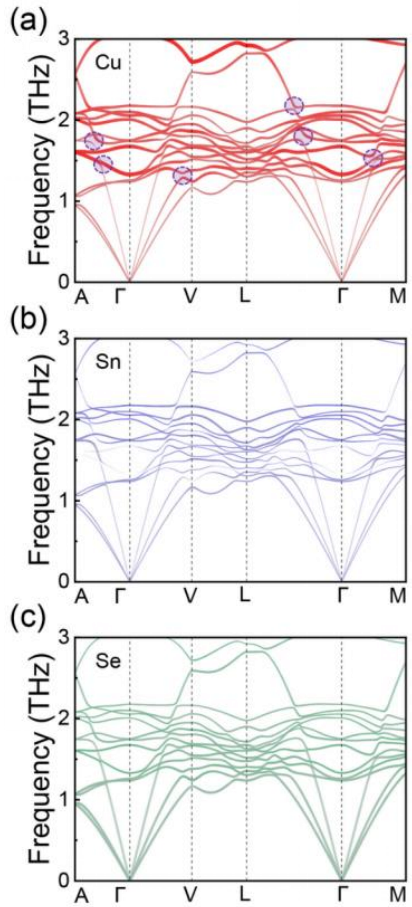

Figure S6. Phonon dispersions of monoclinic Cu_2SnSe_3 weighted by (a) Cu, (b) Sn, and (c) Se.

8. Potential Energy

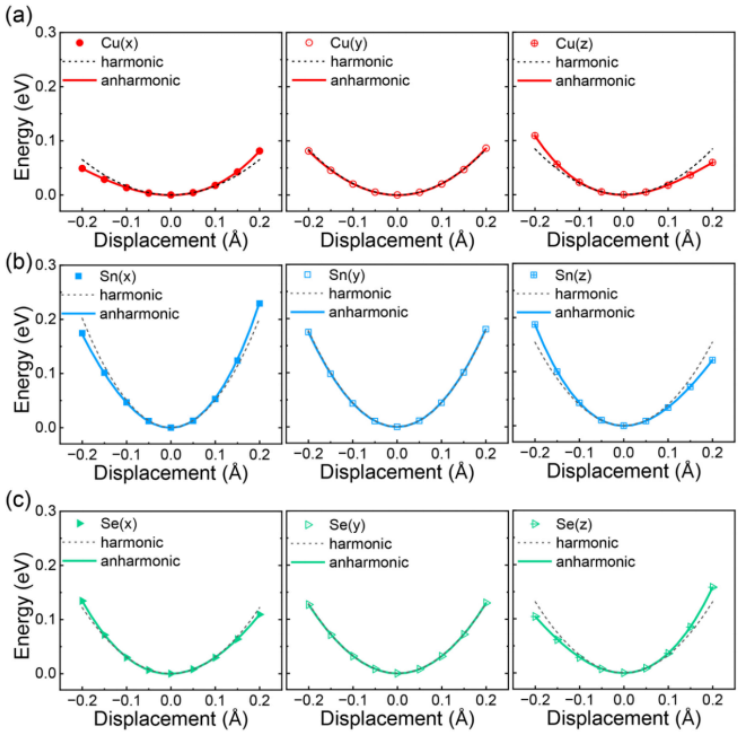

Figure S7. (a) Potential energy of (a) Cu, (b) Sn, and (c) Se in monoclinic Cu_2SnSe_3 along x, y, and z directions.

Tab. S1. Fitting parameters for the potential energy using the polynomial $y=a_1x+a_2x^2+a_3x^3$.

Atoms	**a_1**	**a_2**	**a_3**
Cu (x)	0.0021	1.6298	1.9570
Cu (y)	−0.0046	2.0992	0.4279
Cu (z)	0.0054	2.1074	−3.2172
Sn (x)	0.0051	5.0490	3.5517
Sn (y)	0.0043	4.4441	0.2238
Sn (z)	−0.0037	3.8556	−4.0194
Se (x)	0.0192	3.0496	−2.0507
Se (y)	−0.0048	3.2148	0.3121
Se (z)	0.0041	3.2794	3.2661

9. Crystal Structures of ZnSe, Cu_2SnSe_3, and Cu_2SnS_3

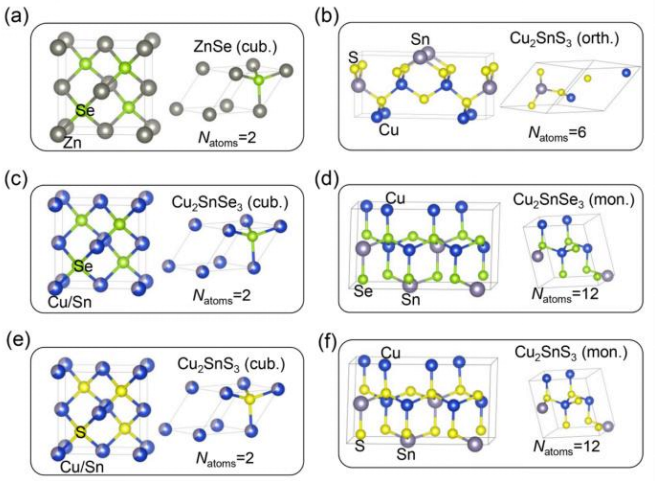

Figure S8. Crystal structures of (a) cubic ZnSe, (b) orthorhombic Cu_2SnS_3, (c) cubic Cu_2SnSe_3, (d) monoclinic Cu_2SnSe_3, (e) cubic Cu_2SnS_3, and (f) monoclinic Cu_2SnS_3.

10. Harmonic Interatomic Force Constants

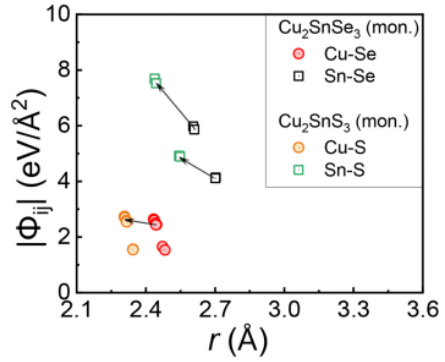

Figure S9. Norm of the harmonic interatomic force constants ($|\Phi_{ij}|$) plotted as a function of the interatomic distance between atoms i and j in monoclinic Cu_2SnSe_3 and Cu_2SnS_3.

References

(1) G. Kresse, J. F. l. Efficient iterative schemes for ab initio total-energy calculations using a plane-wave basis set. *Phy. Rev. B* **1996**, *54* (16), 11169.

(2) Maintz, S.; Deringer, V. L.; Tchougréeff, A. L.; Dronskowski, R. LOBSTER: A tool to extract chemical bonding from plane-wave based DFT. *J. Compu. Chem.* **2016**, *37* (11), 1030-1035. DOI: 10.1002/jcc.24300.

(3) John P. Perdew, K. B., Matthias Ernzerhof. Generalized Gradient Approximation Made Simple. *Phys. Rev. Lett.* **1996**, *77*, 3865. DOI: 10.1103/PhysRevLett.77.3865.

(4) Togo, A.; Tanaka, I. First principles phonon calculations in materials science. *Scripta Mater.* **2015**, *108*, 1-5. DOI: 10.1016/j.scriptamat.2015.07.021.

(5) Momma, K.; Izumi, F. VESTA 3for three-dimensional visualization of crystal, volumetric and morphology data. *J. Appl. Cryst.* **2011**, *44* (6), 1272-1276. DOI: 10.1107/s0021889811038970.

(6) Knoop, F.; Shulumba, N.; Castellano, A.; Batista, J. P. A.; Farris, R.; Verstraete, M. J.; Heine, M.; Broido, D.; Kim, D. S.; Klarbring, J.; et al. TDEP: Temperature Dependent Effective Potentials. *J. Open Source Softw.* **2024**, *9* (94). DOI: 10.21105/joss.06150.

(7) Li, W.; Carrete, J.; A. Katcho, N.; Mingo, N. ShengBTE: A solver of the Boltzmann transport equation for phonons. *Compu. Phys. Commun.* **2014**, *185* (6), 1747-1758. DOI: 10.1016/j.cpc.2014.02.015.

(8) Han, Z.; Yang, X.; Li, W.; Feng, T.; Ruan, X. FourPhonon: An extension module to ShengBTE for computing four-phonon scattering rates and thermal conductivity. *Comput. Phys. Commun.* **2022**, *270*, 108179. DOI: 10.1016/j.cpc.2021.108179.

(9) Balkanski, M. W., R. F. Haro, E. Anharmonic effects in light scattering due to optical phonons in silicon. *Phys. Rev. B* **1983**, *28* (4), 1928-1934. DOI: 10.1103/PhysRevB.28.1928.

(10) Ming, H.; Wang, J.; Xu, S.; Jabar, B.; Zheng, Y.; Luo, Z.-Z.; Zou, Z. Role of Anionic Lone-Pair-Like Electrons in Producing Minimum Lattice Thermal Conductivity. *Phys. Rev. Lett.* **2026**, *136* (23), 236301. DOI: 10.1103/2pdy-5c6k.

(11) Yu, H.; Chen, L.-C.; Pang, H.-J.; Qiu, P.-F.; Peng, Q.; Chen, X.-J. Temperature-dependent phonon anharmonicity and thermal transport in $CuInTe_2$. *Phys. Rev. B* **2022**, *105* (24), 245204. DOI: 10.1103/PhysRevB.105.245204.